Axisymmetric wakes behind a slender body including zero-momentum configurations

Hiroshi Higuchi
Department of Mechanical and Aerospace Engineering, Syracuse University, Syracuse, New York 13244
Toshi Kubota
Graduate Aeronautical Laboratories, California Institute of Technology, Pasadena, California 91125

(Received 10 August 1988; accepted 30 May 1990)

An experimental investigation of turbulent axisymmetric wakes including the zero-momentum case was carried out. Mean and fluctuation velocity profiles were measured and self-similar profiles were observed that decayed very rapidly when the momentum was adjusted to be zero. The wake behavior was found to be sensitive to any small mismatch of momentum and the relaxation zone strongly depended on the intensity and scale of the turbulence in the initial wake.

I. INTRODUCTION

The asymptotic behavior of axisymmetric wakes and jets has been studied both experimentally and analytically in the past, and global parameters such as the mean velocity profile and the wake or jet width can be predicted reasonably well even with a simple eddy viscosity approach. The asymptotic behavior of the axisymmetric wake or jet can be characterized by the initial net momentum (drag of the body or thrust of the jet), and the centerline velocity and the width vary as $x^{-2/3}$ and $x^{1/3}$, respectively, for an axisymmetric wake, and as x^{-1} and x^{1} for an axisymmetric jet. On the other hand, the flow relaxation downstream from the initial region has been found to be strongly dependent on the initial flow conditions, and requires further studies. Bevilaqua and Lykoudis,[1] for example, made a comparative study on the wake development behind two dissimilar axisymmetric bodies with identical drag. Significant differences were noted in the downstream wake developments. The difference in wake behaviors was due to the initial turbulence structures and not the magnitude of the drag commonly used to characterize the wake, which will be discussed later.

Among the wake or jet problems, of particular interest is the case in which the drag of the body is exactly canceled by the strength of the jet. This situation can be found in the wake behind the self-propelled bodies. A simple analysis based on eddy viscosity[2,3] predicts the centerline velocity and the width to vary as $x^{-4/5}$ and $x^{1/5}$. A few experimental investigations have been carried out previously,[4–7] but with the possible exception of Naudascher's experiment,[4] most of the measurements suffer from overly complex initial conditions or do not extend far enough from the body to be able to depict the asymptotic behavior of the wake. Thus an experimental investigation of a turbulent axisymmetric wake with zero-momentum defect was carried out, in which simple but well-defined model geometry and initial conditions were employed, and measurements covered the far wake regions as well as the proximity of the body.

In order to examine the effect of the initial conditions, the drag of a slender body was counteracted with a varying-strength jet to create either an axisymmetric wake, an axisymmetric jet in a cofiowing stream, or a wake of a self-propelled body. Also, the drag of the body was increased by installing roughness elements on the wall. The results are compared with the available computations with different turbulence models.

II. EXPERIMENT

A low-turbulence-level, subsonic wind tunnel was used for this experiment as shown in Fig. 1. The test section is 61 by 61 cm in cross section and 305 cm in length. The bottom wall was adjusted to achieve a zero static pressure gradient in the test section.

A thin-wall tube (2.54 cm outer diameter, 0.71 mm wall thickness) was mounted in the settling chamber to avoid disturbance in the free stream. The length of the model in the test section was 30.5 cm. The most downstream part of the model could be exchanged with other models, such as a rough wall, to study the effect of initial conditions. A controlled amount of air was injected at the open end in the direction parallel to the free stream to balance the drag of the body. Four thin wires within the contraction sections were used to adjust the orientation of the model. Significant efforts were made to establish axisymmetry of the wake over the entire test region. The wake flow is sketched in Fig. 2, together with the nomenclature.

The mean velocity and static pressure measurements were made with a Pitot-static probe connected to a Datame-

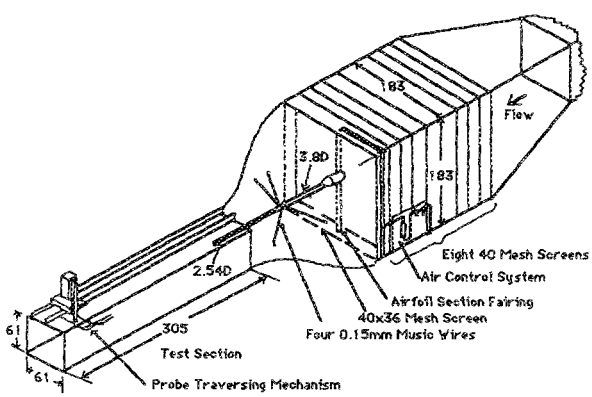

FIG. 1. Experimental setup (units in centimeters).

 0899-8213/90/091615-09$02.00

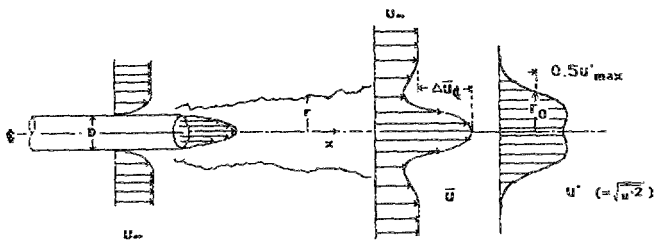

FIG. 2. Definition sketch with the smooth-wall model.

trix type 1014A electronic monometer with a Barocel type 538-10 pressure sensor. The velocity fluctuations were measured with single- and X-wire hot-wire probes connected to a DISA 55A01 constant-temperature anemometer in conjunction with a DISA 55D10 linearizer. The single-wire probe used for the axial velocity fluctuation measurements had a platinum wire 2.54 μm in diameter and 1 mm in length. The frequency response of the system was 16 kHz, and the signal was bandpassed between 5 Hz and 10 kHz before being fed into the DISA 55D35 rms voltmeter and other instruments. The calibration procedure for the hot-wire anemometer system is estimated to be accurate within 2% if the static calibration is assumed to be valid without separate dynamic calibrations. The rms voltmeter was operated with a time constant setting of 0.3 sec, and its dc output was further time averaged by an Interdata model 70 microcomputer. Reynolds stress measurements in a somewhat limited scope were conducted with an X wire with 1.27 μm diameter and 1 mm length. The X-wire signals were digitized and cross-correlated with an A/D converter built at JPL by J. Kendall, Jr. The entire data acquisition was controlled by the Interdata microcomputer. Other details of instrumentation and accuracy of data can be found in Ref. 8.

The free-stream velocity was nominally 16 m/sec and the Reynolds number based on the body diameter was 27 000. The free-stream turbulence was approximately 0.11%.

To visualize the flow, aerosol of dibutyl phthalate was introduced into the wake through the air supply system and was illuminated in the symmetry plane of the wake by the vertical sheet of a laser light produced by passing an 8.5 W argon-ion laser beam through a cylindrical lens. A movie camera was traversed on a carriage alongside the test section to follow the evolution of eddies within the wake. For recording on the film, lower stream velocities (2–7 m/sec) were used, but the main features of the flow were unchanged.

III. RESULTS

The amount of air injection was characterized by the value of the momentum-integral coefficient

$$C_m = \frac{1}{\frac{1}{2}\rho U_\infty^2 (D/2)^2} \int_0^\infty [\rho\bar{u}(\bar{u} - U_\infty) + (\bar{p} - \bar{p}_\infty) + \rho(\overline{u'^2} - \overline{u'^2_\infty})] 2\pi r\, dr,$$

and this integral was numerically computed on an on-line data acquisition system from the mean velocity, mean static pressure, and the axial velocity fluctuation profile measurements. The value $C_m = 0$ corresponds to the zero-momentum case, and without air injection, the drag coefficient of the model C_d is equal to $-C_m$.

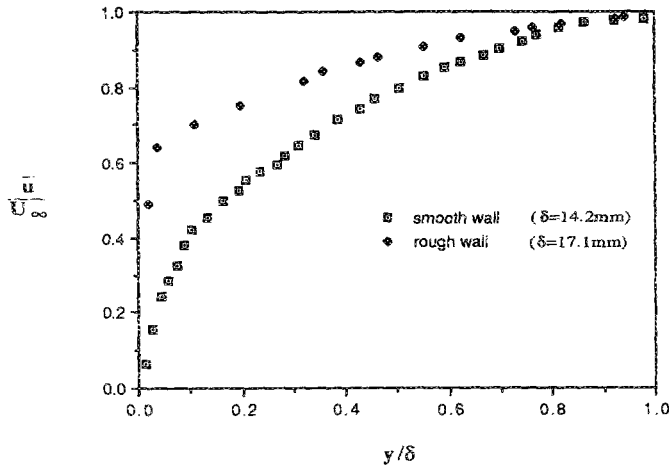

FIG. 3. Boundary-layer velocity profiles on the models.

A. Mean velocity

Both the boundary layer on the model and the jet emerging at the end of the model were found to be axisymmetric, fully developed turbulent flows. Figure 3 shows the boundary-layer profile measured on the exit plane. The figure also includes the profile behind the roughened wall discussed later. The velocity profile of the jet on the exit plane is shown in Fig. 4, where the distance is normalized by the inner radius of the tube. Both velocity profiles of the boundary layer and of the jet followed the established semilogarithmic form.[8]

The mean velocity profile in the pure wake (with no injection) from $x/D = 5$ to $x/D = 89$ is shown in Fig. 5. Normalized by the centerline velocity defect and the half-width, these profiles collapse into a typical Gaussian-like profile. Throughout this paper, the half-width is defined as the radius where the mean axial velocity fluctuation is half of the maximum rms value (see Figs. 2, 6, and 12). (Among various flow configurations tested, the maximum axial ve-

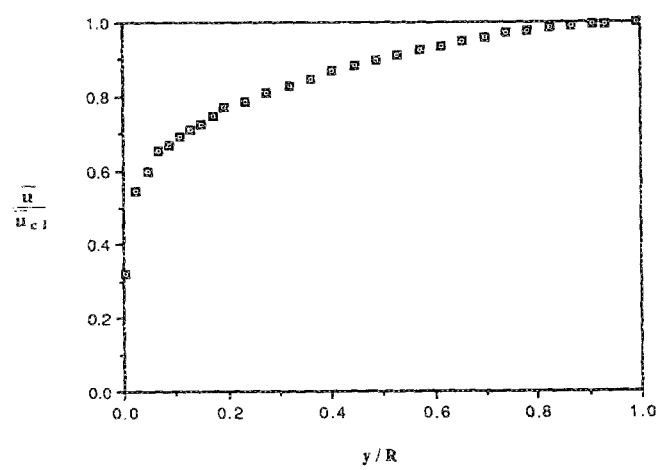

FIG. 4. Mean velocity profile of the jet at the exit.

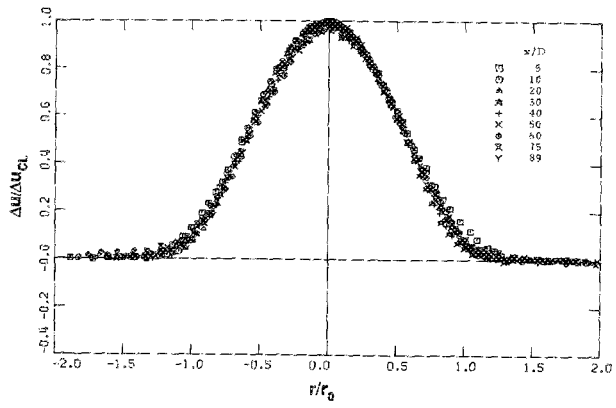

FIG. 5. Pure wake: normalized mean velocity profiles.

locity fluctuation did not always occur on the centerline of the wake, but this definition of the half-width was deemed most applicable to all injection cases that exhibited various mean velocity profiles.) The decay of the centerline velocity defect (Fig. 7) compared well with an established $-\frac{2}{3}$ power law by plotting $(\Delta u)^{-3/2}$ against x, and the growth of the half-width with a $\frac{1}{3}$ power law in a similar manner. The drag coefficient of the body was found to be $C_d \approx 0.68$ from momentum flux measurement.

The jet strength was then adjusted to produce a zero-momentum defect in the matched injection case. Figure 8 shows that the velocity profiles were self-similar when they were normalized by the centerline velocity and the half-width. At a closer inspection, some variations in shape with

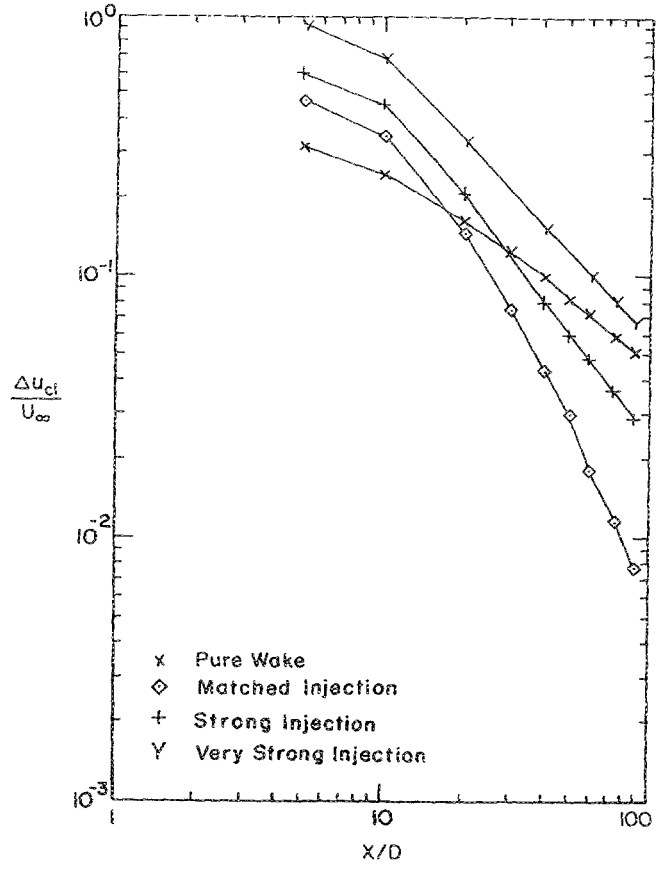

FIG. 7. Axial variation of centerline velocity in various injection cases.

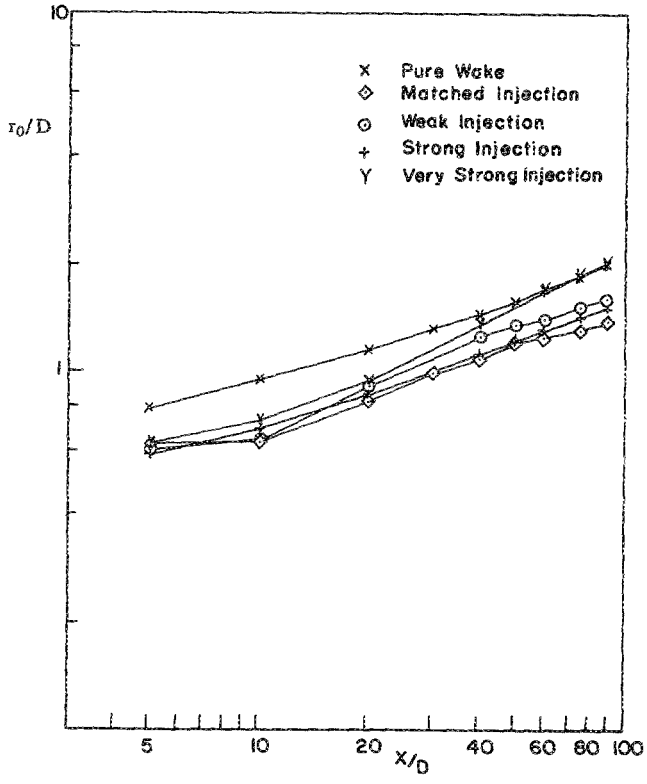

FIG. 6. Spreading of the wake in various injection cases.

the axial position are noticeable, but in consideration of the half-width defined from the turbulence profile and the rapidly decreasing velocity defect, no attempt was made to substantiate the phenomena. The centerline velocity decayed much more rapidly than the $-\frac{4}{3}$ power law predicted by an eddy viscosity model (see, e.g., Tennekes and Lumley[3]) within any reasonable choice of the virtual origin. Figure 9 demonstrates this, as well as the effect of the initial conditions, both of which will be discussed later.

Figure 10 shows the normalized mean velocity profile when the strength of the jet was 40% larger than the drag of

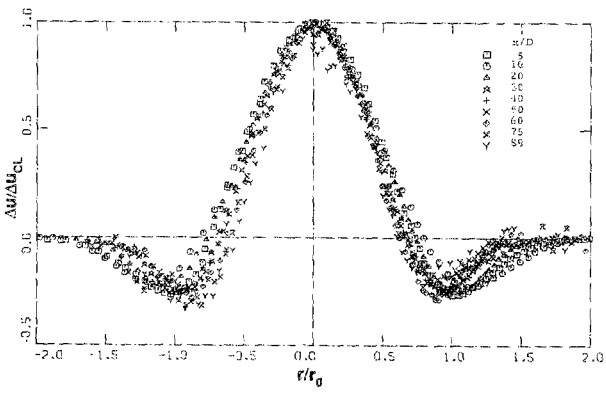

FIG. 8. Matched injection case: normalized mean velocity profiles.

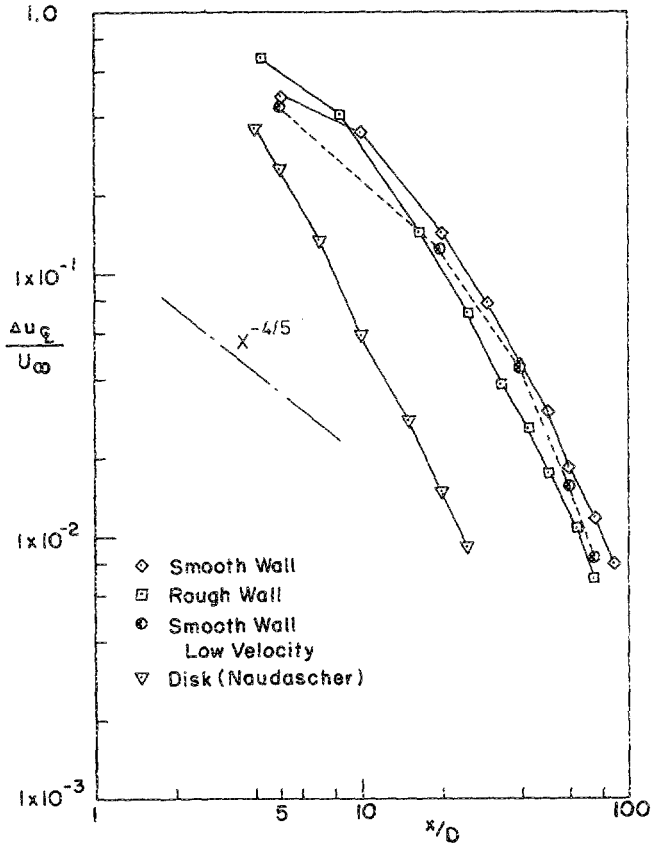

FIG. 9. Axial variation of centerline velocity in matched injection cases.

the body, namely $C_m = +0.4C_d$, where C_d is the drag coefficient of the smooth-wall model. Close to the body, the velocity profiles were similar to those of the zero-momentum case, but farther downstream, the flow relaxed into a self-similar, weak coflowing jet profile, though a slight asymmetry in the profile is noted within the accuracy of measurements. The centerline velocity was plotted in terms of $(\Delta u)^{-3/2}$ vs x. The plot exhibited segmented growth patterns with separate virtual origins, but with appropriate virtual origins, the decay rates agreed with that of a small-increment jet with a $-\frac{2}{3}$ power law. It has been noted, however, that the coflowing jet may not attain a universal similarity with an asymptotic, self-preserving, axisymmetric positive wake.[9,10]

At the strongest injection used in the experiment, the centerline jet velocity at the exit was 2.1 times the surrounding free-stream velocity, and the measurement downstream indicated the excess momentum 2.2 times the pure-wake case. The mean velocity and the velocity fluctuations attained self-similar profiles downstream. Over the distance covered in the experiment, the centerline velocity, $\Delta u_{cl}/U_\infty$ followed a -1 power law with an appropriate virtual origin (see Fig. 7), and the wake did not transition into a self-preserving weak jet farther downstream, which follows a $-\frac{2}{3}$ decay law. (Note that according to Hinze,[10] though universal similarity may not be present, one may expect a transitional region in the coflowing jets where the velocity decay law varies from x^{-1} to $x^{-2/3}$.)

The mean velocity profiles without scaling are presented in Fig. 11 for the case in which the jet injection was slightly weaker than the matched injection case with the momentum defect in the wake equal to 38% of the drag of the model itself (i.e., $C_m = -0.38C_d$). Even though the initial velocity profiles resembled those of the zero-momentum case [Fig. 11(a)], the velocity excess at the centerline decreases and the flow approached the pure-wake profile farther downstream [Fig. 11(b)].

A roughness element was installed on the model which increased drag to a value 1.83 times that of the smooth wall ($C_d = 0.89$ based on a new body diameter). The jet injection was then introduced to cancel this drag. Normalized mean

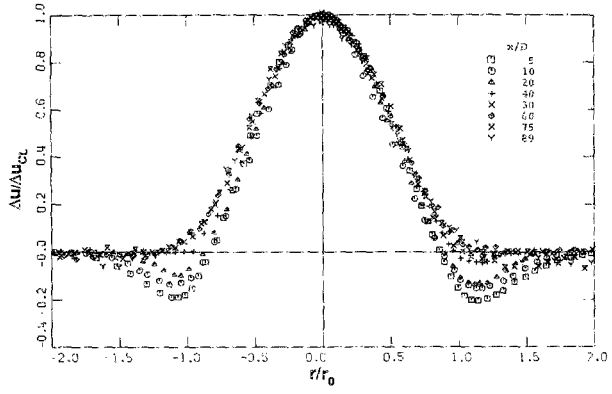

FIG. 10. Strong injection case: normalized mean velocity profiles.

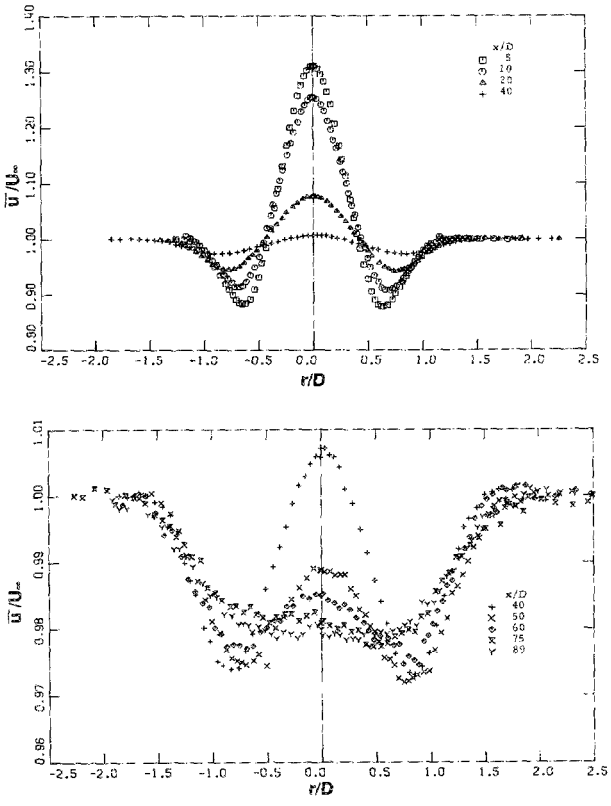

FIG. 11. (a) Weak injection case: mean velocity profiles ($x/D = 5$–40). (b) Weak injection case: mean velocity profiles ($x/D = 40$–89).

velocity and axial velocity fluctuation profiles were found to be of the same shape as in the smooth-wall cases.[8] The centerline velocity decay rates are shown in Fig. 9 together with the smooth-wall case and Naudascher's results[4] behind a circular disk.The centerline velocity shows that the rough-wall case has a shorter relaxation distance prior to the final decay stage as compared with the smooth-wall case. Naudascher's case shows almost no relaxation distance. The figure also shows the matched injection case with a smooth-wall model at a free-stream velocity reduced by half ($Re_D = 13\,400$). The decay rates were very similar to those at the higher velocity.

B. Axial velocity fluctuation

The axial turbulence intensity (rms axial velocity) in the pure wake showed a general self-similar profile. Initial twin-peak profiles at $x/D = 5$ relaxed into the flattop bell-shaped profiles downstream.[8] Uberoi and Freymuth[11] observed a self-similar profile behind a sphere from $x/D = 50$ to 150 and the shape of the profile remains to have twin peaks. On the other hand, the wake behind a slender body (Chevray[12]) exhibited a relaxation process near the centerline of the wake as in the present study, though Chevray's measurements did not extend to the far wake region, his farthest downstream station being $x/D = 18$. The difference from a sphere wake is considered to be due to the persistence of the turbulence structure based on the large-scale vortex shedding from a bluff body. The structure in the far wake, which is traceable to the initial vortex shedding, was observed by Oswald and Kibens[13] in the wake behind a disk.

The radial distributions of turbulence intensity with different jet injection rates were closely self-similar at various axial stations. In addition, the profiles for different injection cases were roughly similar among each other, and thus could be used to define the half-width of the wakes in normalizing the mean velocity profiles as mentioned earlier. The normalized axial turbulence intensity profiles for the matched injection case are shown in Fig. 12 (refer to Ref. 8 for other turbulence profiles). The profiles show a twin-peak humpbacked shape at smaller x/D and relax to a single-peak Gaussian-like distribution.

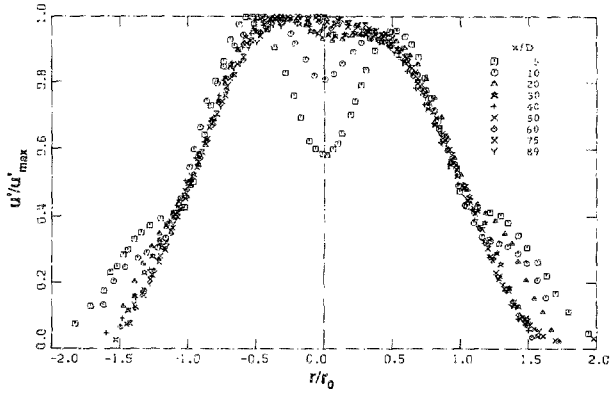

FIG. 12. Matched injection case: normalized axial turbulence intensity profiles.

The power spectra of the axial velocity fluctuations were measured for the pure wake and the matched injection case at various wake positions.[8] The pure wake had a distinct spectral peak (Strouhal number 0.17 based on the body diameter) at the initial region, corresponding to a wave structure seen in the flow visualization. Farther downstream the power spectra exhibited a plateau region with the spectral peak filled in the low-frequency range. The matched injection case, on the other hand, had a broader spectrum at the initial region indicating a more dispersed eddy structure, and downstream, the spectra quickly reached a distribution that decreased monotonically with frequency.

The rates of decay of the turbulence intensity with axial distance differed considerably among the cases as shown in Fig. 13. The results of the pure wake and the very strong injection (essentially a coflowing jet), followed $-\frac{2}{3}$ and -1 power decay laws, respectively. These decay laws matched the respective centerline velocity decay law. The matched injection case and the two unmatched injection cases had faster decay rates than the above two cases. The effect of the different initial conditions on turbulence intensity in the matched injection case is presented in Fig. 14. All the cases in the figure appear to attain a similar asymptotic decay rate with different relaxation distances to their asymptotic stages. We observe that the rough-wall case with a strong jet has a shorter relaxation distance, and the wake behind the disk has the shortest relaxation distance with an initial decay

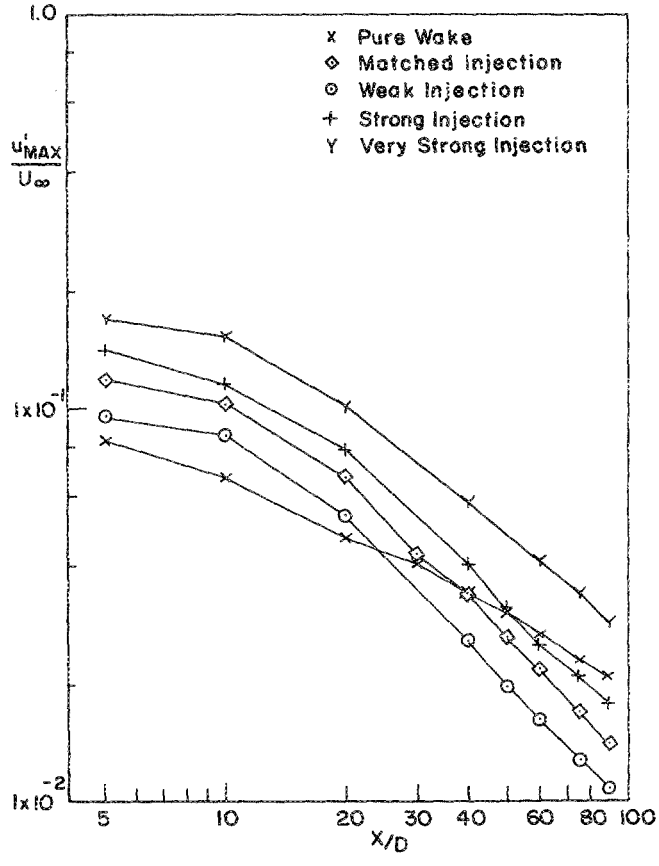

FIG. 13. Axial variation of maximum axial turbulence intensity in various injection cases.

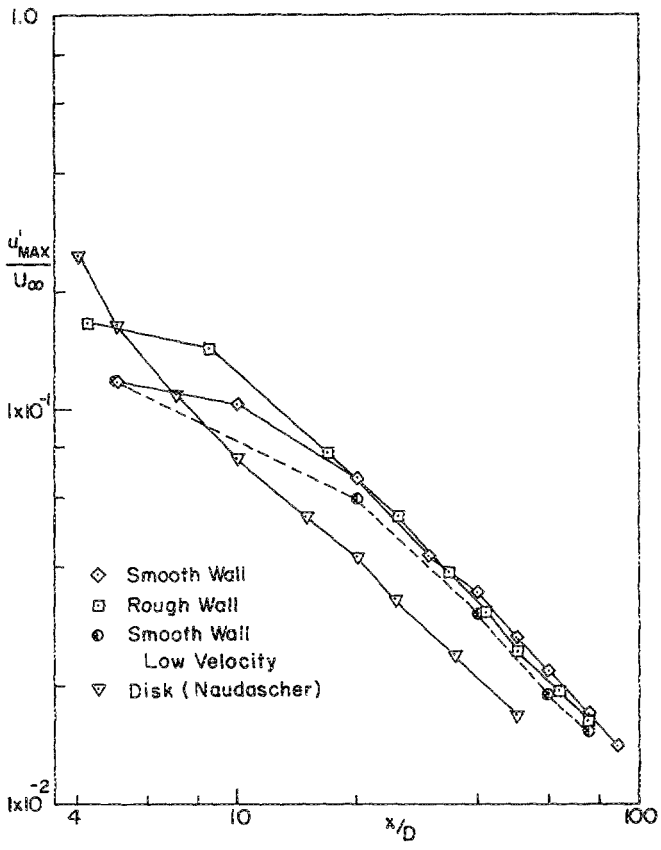

FIG. 14. Axial variation of maximum axial turbulence intensity in matched injection cases.

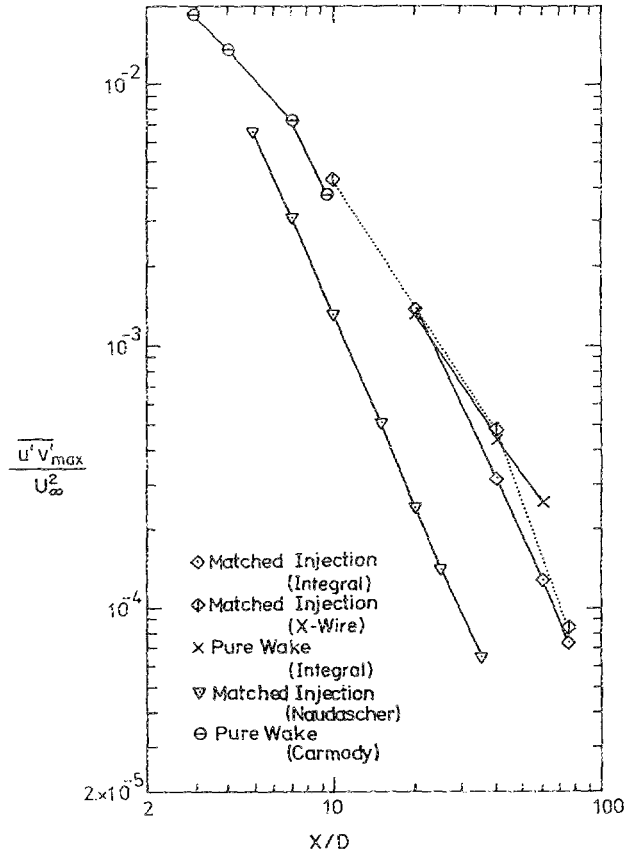

FIG. 15. Axial variation of maximum turbulent shear stress.

rate faster than the asymptotic rate. Between the two smooth-wall cases, the influence of the Reynolds number ($Re_D = 13\,400$ vs $27\,000$) seems to be minimal. The local Reynolds number based on the turbulent velocity, $u'r_0/\nu$, was larger than 500 at the farthest downstream distance in the experiment.

C. Turbulent shear stress

The Reynolds shear stress was computed by integrating the mean momentum equation using the measured mean velocity, static pressure, and axial velocity fluctuation data. Also, the components of the Reynolds stress, $\overline{v'^2}$, $\overline{w'^2}$, and $\overline{u'v'}$, were measured with an X-wire probe at selected axial stations, and the X-wire data agreed with the shear stress from the momentum integral, but with larger scatter.

The Reynolds shear stress profile of the matched injection case has alternating signs that roughly correspond to the derivatives of the mean velocity profiles (see Fig. 8). The axial variations of maximum turbulent shear stress for pure wake and the matched injection case are shown in Fig. 15. The decay rate was similar to the axial component of the Reynolds normal stress $\overline{u'^2}$. Furthermore, it is to be noted that, while decay rates of the centerline velocity were comparable to those of the turbulence intensity in a pure wake and coflowing jet, the velocity decayed much faster than the turbulent intensity in matched and nearly matched (strong and weak injection) cases. This point will be addressed in more detail in the discussions.

D. Flow visualization study

The unique behavior of the matched injection case, compared to those of the more classical pure wake or coflowing jet, was also observed in flow visualizations recorded both on still photos and on the movies in traveling coordinates. In a very weak injection case, which was essentially equivalent to the pure-wake case (except for a minute amount of aerosol being injected for flow visualization purposes), an asymmetric train of eddies traveled downstream and coalescence of neighboring eddies was seen in the intermediate wake region [Fig. 16(a)]. As eddies traveled farther downstream, they grew in size and engulfed the outside flow by their asymmetric vortex motions. An attempt was made to illuminate another plane of symmetry simultaneously, but the exact structure remained unclear, whereas a double-loop structure has been reported[14] behind a sphere.

As the injection rate was increased, the mixing region quickly formed a symmetric train of eddies. These eddies rotated in a direction consistent with the mean velocity gradient. In the strong injection case, large symmetrical eddies rotated in the opposite sense compared with those in the weak injection case as shown in Fig. 16(b). These symmetrical structures of rolling vortices in the symmetry plane in both the weak and strong injection cases appeared like a sliced view of the ring-type vortex structures, though the actual structures are expected to be far more complex in a three-dimensional manner as discussed by Perry *et al.*[15]

Immediately noticeable in the photos and the movie following the wake of the matched injection case was its lack of

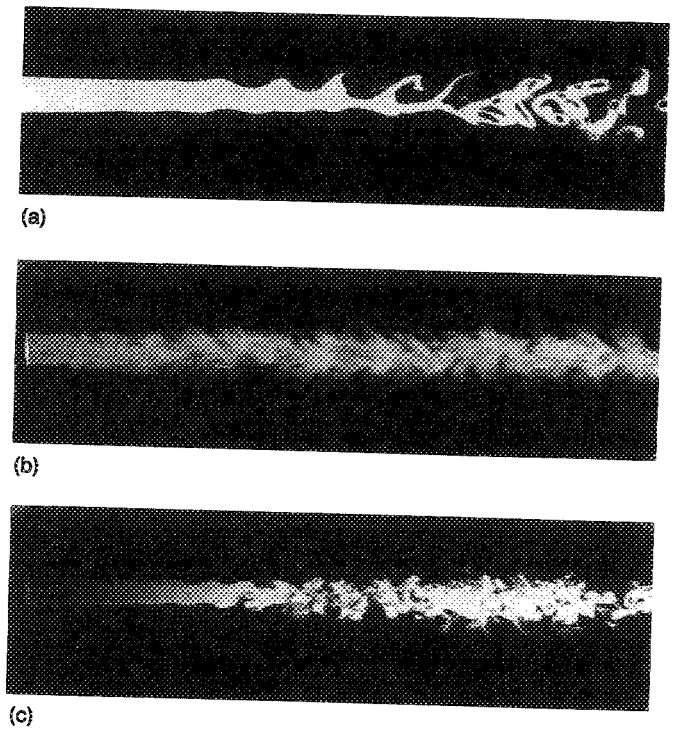

FIG. 16. Laser sheet smoke flow visualizations ($Re_D = 2620$, $x/D = 0$–20). (a) Very weak injection; (b) strong injection; (c) matched injection.

organized large-scale eddy rotations [Fig. 16(c)]. At a higher Reynolds number, the wake contained a finer structure of eddies, but the global structure was independent of the Reynolds number. Close to the exit of the model, a high degree of eddy motions was present in the jet, but they rapidly broke up and subsequently eddies diffused outward as they were convected downstream without preferred rotations. Mushroom-shaped eddies were characteristic of this wake, and they were also seen diffusing outward. In addition, the center region became more intermittent downstream, possibly indicating the penetration of the potential flow region into the wake. Intermittency factor measurements by the hot-wire probe supported this observation.

IV. DISCUSSION

A. Equilibrium between mean flow and turbulent flow

Townsend[16] first investigated the wake of a circular cylinder and concluded that it takes in excess of 1000 diameters before the total kinetic energy of the turbulent motion and the total kinetic energy of the mean flow reach a complete equilibrium. (The similarity solution of a two-dimensional far wake was recently reexamined by Hariri *et al.*[17]) The present study indicated that the process of approaching the asymptotic behavior is dependent on the initial condition, particularly on the shape of the body. It is therefore of interest to investigate the existence of and the process of obtaining the equilibrium between the mean flow and turbulent flow. This was first carried out in the pure wake with various conditions. It is assumed that the turbulent motion is characterized by the maximum axial turbulent intensity and the mean flow motion by the centerline velocity defect. If the axial turbulent intensity is proportional to the total turbulent energy, this ratio becomes a square root of the ratio between turbulent energy and the total mean energy as used by Townsend.[18] The ratio formed by these two parameters is plotted in Fig. 17. It is immediately noticeable that the wake behind the slender bodies[7,12] does not attain equilibrium even at 40 diameters downstream, whereas the wake behind bluff bodies such as a disk[19] and sphere,[1,11] exhibit the constant value of the ratio much closer to the body. The present results behind a smooth-wall model and behind a rough-wall model show a more gradual increase in the ratio than those behind a spheroid or a slender body. The ratio, nevertheless, has not attained an asymptotic value at the farthest downstream station, possibly indicating the flow to be still approaching equilibrium. Behind the bluff bodies the ratio between the maximum axial turbulent intensity and the centerline velocity defect attain the value 0.9–1.0. The wake behind the spheroid or the slender body shows steady increase up to the farthest downstream measurements, and it needs to be seen if the wake could be developing to reach similar values. It is to be noted that behind a porous disk[1] this ratio between turbulence and mean flow reaches an asymptotic value at a relatively short distance from the body, but its value is significantly lower. Bevilaqua and Lykoudis[1] reported the slower development of the wake behind the porous disk as compared to the wake behind a sphere having the same drag, and it remains to be seen if a universal ratio exists for axisymmetric wakes.

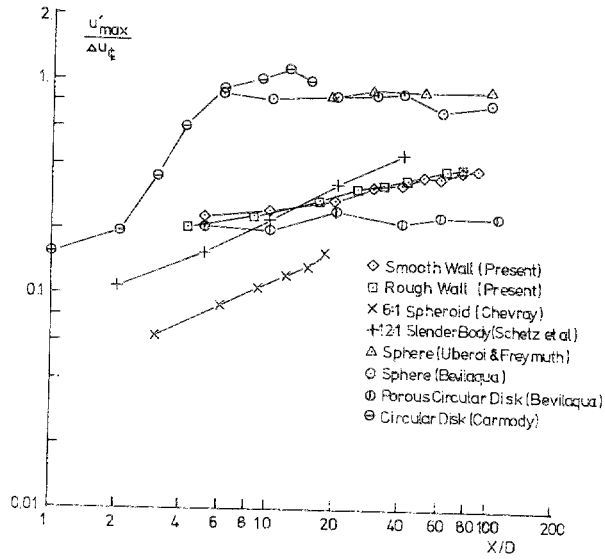

FIG. 17. Balance between mean flow and turbulence in pure wakes.

In the matched injection case, the ratio between the axial turbulence intensity and the maximum velocity difference, $\Delta u_m = u_{max} - u_{min}$, was calculated and compared with other injection cases in Fig. 18. In the pure wake, strong injection and very strong injection cases, the ratio very gradually increases. In the four matched injection cases the ratio behaves differently from the above three cases, showing a steady rapid increase in value downstream. Clearly the equilibrium does not exist between the mean velocity difference and the turbulent velocity fluctuation in these flows. In the weak injection case, as discussed earlier, u_{max} is equal to

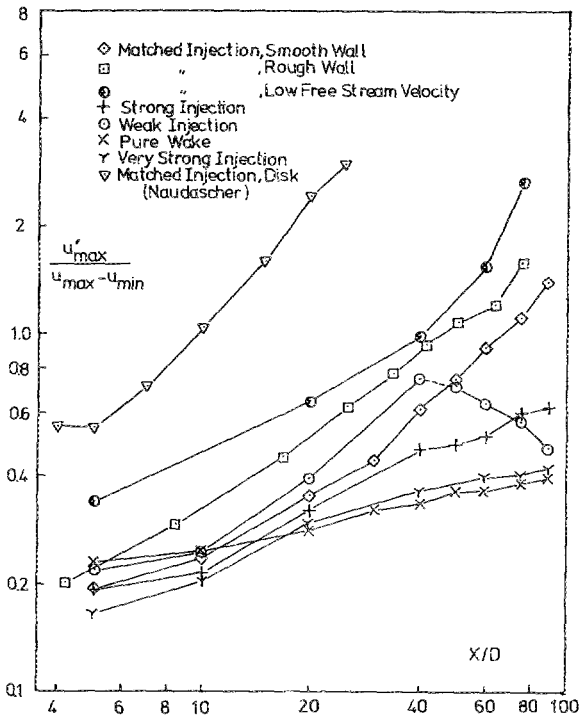

FIG. 18. Balance between mean flow and turbulence in various injections.

u at the centerline for $x/D < 40$ and the ratio increases in a similar manner as the matched cases. Beyond $x/D = 40$, u_{max} is equal to the free-stream velocity and the ratio tends toward a pure-wake value.

The ratio between the maximum turbulent shear stress and the centerline velocity defect is plotted in Fig. 19. This ratio indicates a ratio between the dissipation and the production of turbulent energy (e.g., refer to Ref. 18). The results resemble those in Fig. 18 as expected, since the experimental data showed that the ratio of maximum shear stress $\overline{u'v'_{max}}$ and the maximum axial velocity fluctuation $\overline{u'^2_{max}}$ was relatively constant. The steady increase in the ratio $\overline{u'v'_{max}}/(\Delta u_{cl})^2$ in the matched injection case illustrates that the rate of production becomes less important in the turbulent energy budget. Between two matched injection cases shown, the ratio in the smooth-wall case is significantly lower than that in the wake behind the disk reflecting the different mechanisms of initial turbulence generation in these cases. Disparities among the asymptotic ratios behind axisymmetric pure wakes are also seen.

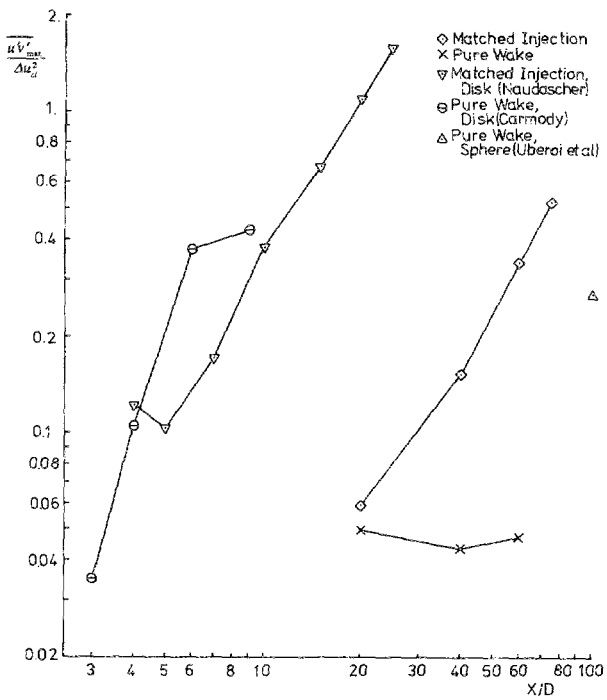

FIG. 19. Ratio between maximum turbulent shear and centerline velocity defect.

B. Effect of the initial condition

The effect of the initial boundary layers on the model was investigated with the roughness element on the model wall, which produced a drag 1.83 times that of the smooth wall, as stated earlier. The jet injection was readjusted accordingly to produce the zero-momentum wake. As shown in Figs. 9 and 14, the mean velocity and the turbulence intensity approached the downstream decay region nearly three times sooner. Naudascher's result behind a solid disk shows a still faster approach to the final decay rate. These results may be interpreted qualitatively as follows. For the present smooth-wall body, turbulent boundary-layer flow and jet flow, both fully developed, merge at the end of the thin-walled tube. Relatively small-scale eddies that are in equilibrium themselves merge together, and the eddies must adjust their size to a scale that is compatible with the wake width before the flow establishes asymptotic behavior as a fully developed free-shear layer. On the other hand, the momentumless wakes behind the rough-wall model or a bluff body like the circular disk reach their final stage sooner because the turbulence intensity is higher, and because the initial eddy sizes are larger and closer to those of the far wake. This notion is also consistent with the result of Bevilaqua and Lykoudis on regular momentum wake[1] which reported a slower development of the wake behind the porous disk than that behind a sphere with the same drag. This requires a further study, however, which should include more detailed data such as the integral length scale distribution in the wake.

C. Comparison with the analysis

In the past, the simple eddy viscosity models, such as Prandtl's free-shear flow model or mixing-length model, have predicted the behavior of various free-shear flows reasonably well, including pure wakes and coflowing jets. However, the results of a model with eddy viscosity constant across the wake as given in Birkhoff and Zarantonello[2] and Tennekes and Lumley[3] failed to predict that of a zero-momentum wake and other relaxing flows. Though the normalized velocity profile was similar to that observed, it was clearly shown from a measured rapid velocity decay rate of the matched injection case that the classical eddy viscosity model failed to predict the momentumless wake by a wide margin (see Fig. 9). The fault of the analysis stems from the assumption in the Reynolds stress. The similarity form used

for the eddy viscosity model, $\overline{u'v'} = (\Delta u_{cl})^2 g(\eta)$, is equivalent to the assumption $\overline{u'v'_{max}}/(\Delta u_{cl})^2 = \text{const}$. The values of this constant can be found in Tennekes and Lumley[3] or Townsend[18] for self-preserving wake flows. As shown in Fig. 19, this assumption appears to be verified in the present pure wake, but the experimental results for the matched injection case indicates that the ratio is far from constant. Equilibrium between production and dissipation of energy has been the underlying principle of eddy viscosity models.

Finson[20] kept the turbulence intensity term in the momentum balance, and neglected the production term from the energy equation while retaining it in the shear stress equation. He obtained decay laws on the mean velocity, turbulent intensity, Reynolds stress, and wake width (for example, $x^{-18/11}$ for the mean velocity) close to Naudascher's data. His result also compared fairly well with the present results, though different virtual origins were required for different quantities. Metcalfe and Riley[21] conducted a direct numerical simulation of the present matched injection case using nonsteady Navier–Stokes equations and a set of experimental data as initial conditions. Though the method appeared to give better results in the nonzero net momentum case, the turbulent intensity and the shear stress variations were predicted well and the mean velocity decay was also predicted reasonably well even in the momentumless wake. These results affirmed the importance of taking the detailed interaction among the turbulence quantities and mean flow into account in predicting the momentumless wakes.

V. CONCLUSION

The present study has produced the following results.

(1) A self-similar velocity profile in momentumless wakes was observed, and the self-similarity was found to be extremely sensitive to the balance of the momentum flux in the wake.

(2) The centerline mean velocity defect in the zero-momentum cases decayed at a much higher rate than in the pure wake or in the strong injection cases. The effects of zero-momentum defect on the decay rate of turbulence intensity and the wake spreading rate were much smaller than the effect on the mean velocity.

(3) The relaxation length in which the momentumless wake reaches its final stage depended on the initial conditions. The momentumless wakes behind the rough-wall model or a bluff body like the circular disk reached their final stage sooner because the turbulence intensity is higher, and because the initial eddy sizes are larger and closer to those of the far wake.

(4) The flow visualization in the symmetry plane showed in the pure wake and in the strong and weak injection cases, the large eddy rotations engulfing the potential flow. The rotations were in the same direction as the mean vorticity of the flow. In the momentumless case, on the other hand, these large eddy rotations were absent and increasing folding of the interface of the turbulent region and the resulting larger intermittency were observed downstream.

(5) Simple modeling of the Reynolds stress, such as Prandtl's eddy viscosity model, fail to predict accurately the momentumless wake, mainly because the equilibrium between production and dissipation of turbulent energy, which is an underlying principle in simple turbulence modeling, is absent in the momentumless wakes. The Reynolds shear stress cannot be described only by the mean flow quantity, and it is essential that a model include the mechanism of the balance of the turbulent stresses in order to describe these wakes satisfactorily.

ACKNOWLEDGMENTS

The authors wish to express their gratitude to Dr. J. M. Kendall, Jr. and Dr. D. J. Collins of the JPL for their help during the experiment.

[1] P. M. Bevilaqua and P. S. Lykoudis, J. Fluid Mech. **89**, 589 (1978).
[2] G. Birkhoff and E. H. Zarantonello, *Jets, Wakes and Cavities* (Academic, New York, 1957).
[3] H. Tennekes and J. L. Lumley, *A First Course in Turbulence* (MIT Press, Cambridge, MA, 1972), pp. 124–127.
[4] E. Naudascher, J. Fluid Mech. **22**, 625 (1965).
[5] A. S. Ginevskii, K. A. Pochikina, and L. N. Ukhanova, Izv. Akad. Nauk. SSSR Mekh. Zhidk. Gaza **1**, 164 (1966).
[6] R. L. Gran, TRW Systems Report. No. 20086-6006-RU-00, 1973.
[7] J. A. Schetz and A. K. Jakubowski, AIAA J. **13**, 1568 (1975).
[8] H. Higuchi, Ph.D. thesis, California Institute of Technology, 1977.
[9] R. A. Antonia and R. W. Bilger, Aeronaut Q. **25**, 69 (1974).
[10] J. O. Hinze, *Turbulence* (McGraw-Hill, New York, 1975), 2nd ed.
[11] M. S. Uberoi and P. Freymuth, Phys. Fluids **13**, 2205 (1970).
[12] R. Chevray, J. Basic Eng., Trans. ASME D **90**, 275 (1968).
[13] L. J. Oswald and V. Kibens, Department of Aerospace Engineering Technical Report No. 002820, University of Michigan, 1971.
[14] H. P. Pao and T. W. Kao, Phys. Fluids **20**, 187 (1977).
[15] A. E. Perry, T. T. Lim, and M. S. Chong, J. Fluid Mech. **101**, 243 (1980).
[16] A. A. Townsend, Proc. R. Soc. London Ser. A **190**, 551 (1947).
[17] A. Hariri, P. A. Libby, and J. C. LaRue, Phys. Fluids **25**, 1964 (1982).
[18] A. A. Townsend, *The Structures of Turbulent Shear Flow* (Cambridge U. P., Cambridge, 1976), 2nd ed.
[19] Y. Carmody, J. Basic Eng., Trans. ASME D **86**, 869 (1964).
[20] M. A. Finson, J. Fluid Mech. **71**, 465 (1975).
[21] R. W. Metcalfe and J. J. Riley, Flow Research Note No. 193, Flow Research Company, 1981.